VOL. 20, NO. 2-2, 2021, 15-19
www.elektrika.utm.my
ISSN 0128-4428

ELEKTRIKA
Journal of Electrical Engineering

Finite Element Analysis of Material Removal Rate for Si Wafer using Heat-assisted µEDM

Noor Dzulaikha Daud[1], Marwan Nafea[2] and Mohamed Sultan Mohamed Ali[1]*

[1]School of Electrical Engineering, Faculty of Engineering, Universiti Teknologi Malaysia, 81310 UTM Johor Bahru, Johor, Malaysia
[2]Department of Electrical and Electronic Engineering, Faculty of Science and Engineering, University of Nottingham Malaysia, 43500 Semenyih, Selangor, Malaysia

*Corresponding author: sultan_ali@fke.utm.my

Abstract: Micro-electrical discharge machining (µEDM) has been proved to produce high surface quality results in Si machining. In previous studies, the researchers reported the Si machining using the µEDM with several strategies such as plating, doping and temporary coating process to be machined by the µEDM. This paper reports a numerical simulation of MRR performance results using COMSOL Multiphysics. The effects of the machining temperature in Si machining using heat-assisted µEDM on achieving the optimum MRR results is studied. The simulation results showed the highest MRR is 1.48666 $\times 10^{-5}$ mm^3/seconds achieved at 250 °C.

Keywords: Heat-assisted µEDM, Machining, Material removal rate, Numerical simulation, Silicon wafer.

Article History: received 25 May 2021; accepted 12 June 2021; published 15 September 2021.

1. INTRODUCTION

Si wafers is a superior material that easily to control precisely its mechanical and electrical properties [1, 2]. Moreover, the Si is known as a hard to machine materials due to its high brittleness [3]. As a result, in chemical etching process, the Si machining is limited to two-dimensional only. Most of the microelectromechanical system (MEMS) devices and applications required a three-dimensional (3D) microstructures which enables by non-conventional machining techniques such as ultrasonic, ion-milling and laser beam to address the limitations of the chemical etching. However, these techniques cause thermal damage [4], crack formation [5] and resulted in low material removal rate (MRR) [6]. The µEDM is one of non-conventional machining techniques to machine structures of Si wafer regardless of its crystal orientation [7] and hardness [8]. The µEDM is widely used on conductive materials and also applicable to the non-conductive materials like semiconductors [9] and ceramics [10]. The researchers reported on the Si machining using the µEDM with the assisted of plating [11], doping [12] and coating [13] process to change the Si to become conductive before being machined by the µEDM. These techniques caused the changes of Si material properties. The new develop machining techniques, heat-assisted µEDM has been introduced by Daud *et al.* [14] which applied the heating temperature to the Si wafer to change its electrical conductivity and enable the machining process. The machining temperature have been applied in five different temperature to study the effect of conductivity to the µEDM machining performances.

This paper proposes numerical simulation of the multi-spark to design a model for the heat-assisted µEDM process, and to analyze the MRR performances. A heat transfer module in the COMSOL Multiphysics 5.5 was used to develop the numerical simulation of the single, or multi-spark model of the heat-assisted µEDM process and MRR. The following sections discuss the model's description, assumptions, and results of the simulation that were implemented using the COMSOL Multiphysics software.

2. NUMERICAL SIMULATION OF MRR DESIGN

The designed model could estimate the cavity depth, cavity volume, and temperature distribution of the workpiece's surface during the machining process, depending on the parameter settings, as per Table 1. Figure 1 shows the 2D physical domain to be used for a single spark simulation. The multi-spark simulation also used the same physical domain, except that the location of the sparks were from initial to final locations, compared to the fixed position of the single-spark simulation.

Table 1. Parameter settings used in the simulation.

Parameter settings (simulation)	Value
Spark radius, R_{sp} (tool radius)	150 µm

Spark duration (pulse-on time), t_d	30 µs
Melting temperature, T_m	1414 °C
Density, D	2330 kg/m^3
Heat fusion	1787 kJ/kg
Open-circuit voltage, V	100 V
Capacitance, C	10 nF
Discharge energy, DE	$0.5 * C * V^2$
Proportion of discharge energy per pulse, η	0.39
Heat flux, q_w	$4.5 * \eta * E / (t_d * \pi * R_s^2)$
Ambient temperature, $T_\circ$	250 °C

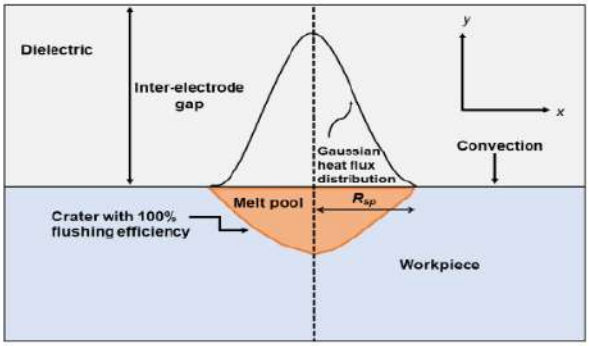

Figure 1. Schematic diagram of single spark of µEDM.

2.1 Assumptions

The simulation model aimed to predict the fundamental parameter for the µEDM process, which is the MRR. There are some assumptions which were considered in the COMSOL Multiphysics simulation, to simplify the modeling process. In this numerical simulations, the following assumptions were considered [15]:

1. The Electrode's surface is initially flat.
2. The electric field's intensity between the electrodes are influenced directly by the inter-electrode gap, as the dielectric, which is free of impurities, reionizes completely after a discharge.
3. A single discharge results from a single electrical pulse input.
4. The conduction process is essential for the heat transfer to the workpiece, and the DE is constant at the workpiece for a fixed parameter setting.
5. The workpiece material is assumed to be homogeneous and isotropic. The thermophysical properties of the workpiece are temperature independent.
6. The DE is assumed to be at a maximum value.

2.2 Simulation model

The heat conduction equation involved the fraction of the DE to the workpiece, which is applied onto the bulk material. The boundary conditions receive the heat flux according to the Gaussian distribution of the input energy for the distance of the heat source from the center, x, which is less than the radius of the spark, R_{sp}. The effect of the conduction heat is melting and evaporation of the workpiece material. The heat conduction equation is expressed in Equation (1):

$$\frac{\partial}{\partial x}\left(K_t \frac{\partial T}{\partial x}\right) + \frac{\partial}{\partial y}\left(K_t \frac{\partial T}{\partial y}\right) + \frac{\partial}{\partial z}\left(K_t \frac{\partial T}{\partial z}\right) = D \cdot C_p \cdot \frac{\partial T}{\partial t} \quad (1)$$

where, x, y and z are the coordinates of the cylindrical work domain, T is the temperature, K_t is the thermal conductivity, D is the density, and C_p is the specific heat capacity of workpiece material.

The boundary conditions during the pulse-on time are expressed in Equation (2):

$$-K\frac{\partial T}{\partial y} = \begin{cases} q(x), & x \le R_{sp} \\ h(T_s - T_0), & x > R_{sp} \end{cases} \quad (2)$$

where, T_s and T_0 are the temperatures of the workpiece adjacent to the cavity boundary and the ambient temperature, and h is set at 10 W/m^2, which represents the convective heat transfer coefficient.

The heat q_w is the Gaussian distribution of the heat flux proposed by Patel *et al*. [16] to predict the heat value to the workpiece and the maximum heat flux, $q_\circ$ which is expressed by:

$$q_w(x) = q_0 \cdot exp\left\{-4.5\left(\frac{x}{R_{sp}}\right)^2\right\} \quad (3)$$

Equation (4) shows the empirical equation, which is the approximate radius expanded with the pulse-on time:

$$R_{sp} = 0.0284(t_d)^{0.9115} \quad (4)$$

where, t_d represents the pulse duration (pulse-on time) in microseconds, V is the open-circuit voltage, and I is the discharge current (A). The maximum heat flux, q_0 (W/m^2) at $x = 0$ is calculated using the following equation:

$$q_0 = 4.5\left(\frac{\eta \cdot E}{t_d \cdot \pi \cdot R_{sp}{}^2}\right) \quad (5)$$

where, η is 0.39, which represents the proportion of the DE per pulse, distributed to the workpiece and the present model. The DE per pulse, E, is expressed by the following Equation (6):

$$E = \frac{1}{2} \cdot C \cdot V^2 \quad (6)$$

where, C is the capacitance value, and V is open-circuit voltage. For the thermal ablation model, the thermal conduction of the incident heat flux to the workpiece increases, which is caused by the cavity to the form, because of the melting and partial evaporation process. The thermal ablation model assumes that when the

temperature of the material exceeds the melting point, the flushing efficiency is completely removed from the cavity. In a real situation, the molten material is swept away by the dielectric fluid, which is defined as the convective heat flux in the numerical simulation. During the pulse-off time, the cavity is expressed according to the following Equation [17]:

$$-K\frac{\partial T}{\partial y} = q_a = h_a(T_m - T_0) \qquad (x \le R_{sp}) \qquad (7)$$

where, q_a is the convective heat flux (W/m^2), T_m is the melting temperature, T_o is the ambient temperature which is equal to 250 °C (change based on heater's temperature), and h_a represents the temperature dependent convective heat transfer coefficient. In this model, the temperature-dependent is considered for the deriving the convective heat transfer coefficient. The value of h_a is defined as follows:

$$h_a = \begin{cases} 0, & T < T_m \\ h_a \propto T, & T \ge T_m \end{cases} \qquad (8)$$

The volume of material in the cavity above the melting temperature releases heat because through convection, which is the same as that of the convective heat flux. The normal convective velocity, V_a, is the rate required to generate a cavity using a solid boundary, under the influence of the heat flux erosion, which is defined as follows:

$$V_a = \left(\frac{q_a}{D \cdot H}\right) \qquad (9)$$

where, H represents the latent heat of the melting (kJ/kg) and D is the density of the workpiece (kg/m^3).

3. RESULTS AND DISCUSSION

This section presents the numerical simulation of the heat-assisted µEDM using the thermal conduction and thermal ablation model. The physical properties of the Si wafer (n-type; resistivity 1-10 Ω.cm) from the heat transfer module in the COMSOL Multiphysics 5.5, were used as workpiece properties in this simulation. The tool size of the brass material with 300 µm in diameter was used to machine a 100 µm depth for each cavity. The parameter settings concerning the resistance-capacitance (*R*-*C*) circuit in this study were 100 V and 10 nF, resulting in a value of 50 µJ. The *R*-*C* fundamental circuit equations determine the charging time or pulse-off time, which is assumed as the pulse-on time (discharge time) which is half of the pulse-off time. For machining of the workpiece, different temperature ranges of 30, 50, 100, 150, 200 and 250 °C were applied to the Si workpiece. By applying the Gauss distribution of the heat flux input to the workpiece, the cavity diameter and depth were formed. Figure 2 shows the details of the temperature distributions on the machined cavities at 200 °C. The temperature scale represents the steady-state temperature of the workpiece after the removal of the molten liquid.

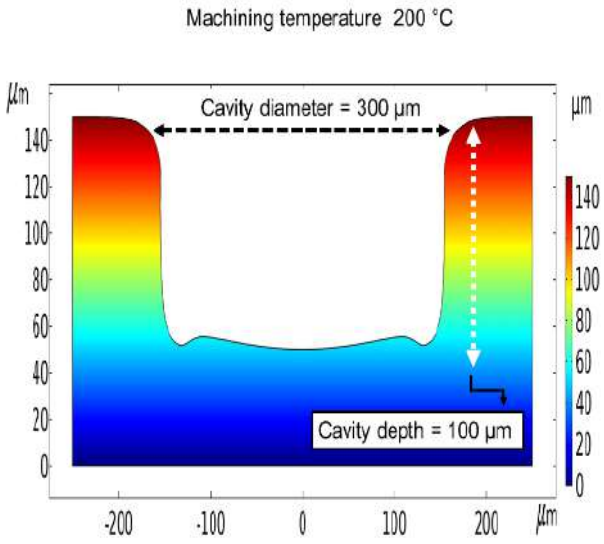

Figure 2. Simulated of finished multi-spark cavity at 200 °C.

In this study, the numerical simulation for a single-spark, i.e., the variation of the cavity depth influenced by the applied temperature to the workpiece was studied. Figure 3 shows the simulation results of the cavity depth vs the machining time. The cavity depth shows an increasing trend due to the increasing temperature, which allows the sparks to remove the material during the machining process. This trend is similar to that of the other three temperatures, as shown in Figure 3.7a-c. In terms of material removal, when the applied temperature increases in the machining process, the volume of material removed per pulse increases. The increment of the volume of material due to the applied temperature changes the Si's conductivity levels to enable a higher machining rate. Figure 4 shows the machined volume against time at three different temperatures, i.e., 50, 150 and 250 °C. The temperature effects the depth and machined volumes of the cavities, thus, the cavity's depth and machined volume increases with an increase in the temperature of the workpiece. Table 2 shows the volume of the machined Si across all six temperatures, which represents an increment with time.

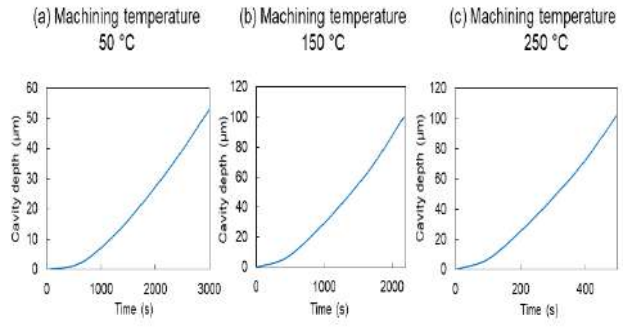

Figure 3. Relationship of cavity depth and machining time (a) 50 °C (b) 150 °C and (c) 250 °C.

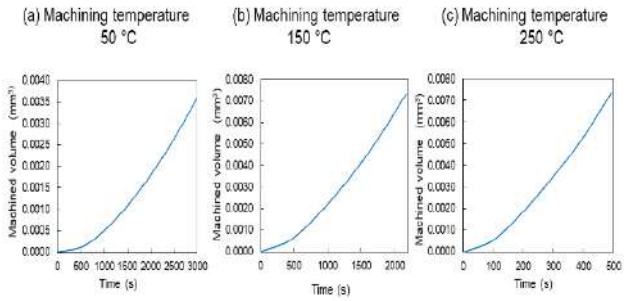

Figure 4. Machined volume (simulation) at (a) 50 °C (b) 150 °C and (c) 250 °C.

Table 2. Simulation results of machined volume and MRR.

Temperature	Machined	MRR (mm^3/sec)
30	1.9085×10^{-3}	6.36167×10^{-7}
50	3.6175×10^{-3}	1.20583×10^{-6}
100	7.2759×10^{-3}	2.79842×10^{-6}
150	7.3294×10^{-3}	3.37294×10^{-6}
200	7.3463×10^{-3}	7.50388×10^{-6}
250	7.3441×10^{-3}	1.48666×10^{-5}

Additionally, the single-spark typically lacks an unavoidable phenomenon, such as the precise position of the spark's occurrence, exact cavity overlap between two adjacent cavities, and the rate of machining for a single layer removal. In the single-spark simulation, the diameter of the cavity and the total time for the single-spark is used to calculate the number of sparks, and the total machining time. However, to study the machined surface, the machining surface characteristics need to be analysed in the multi-spark machining. This is because of a high frequency of the multi-spark, which presents spark erosions at multiple points on the workpiece, one after the other. Using the COMSOL Multiphysics 5.5, the heat transfer module, the position, and the duration of the spark were controlled. The total machining time, which is similar to the simulation time, was evaluated by the total number of sparks, and the total time of a single-spark. Thus, in this study, the multi-sparks were evaluated and summarized based on three temperatures: 50, 150 and 250 °C. Figure 5 illustrates the 2D surface of cavity depth based on the percentage of the total machining time. After 25, 50, 75 and 100 %, the cavity's depth profile is shown in Figure 5(a)-(d), respectively. In the early phase of the cavity's depth, 25 % of the total machining time can be observed in Figure 5(a). The final workpiece's surface depth is shown in Figure 5(d). By applying heat to the workpiece, the removal layer is machined layer-by-layer from the Si workpiece to reach the required depth. The temperature profile of 50 % (Figure 5(b)) and 75 % (Figure 5(c)) show the machining depth after half and three-quarter of the total machining time. Based on the simulation results, at the temperature of 50 °C, the final cavity depth is removed to about 50 µm only (150 – 100 µm), which indicates that the temperature of 50 °C is not sufficient for µEDM.

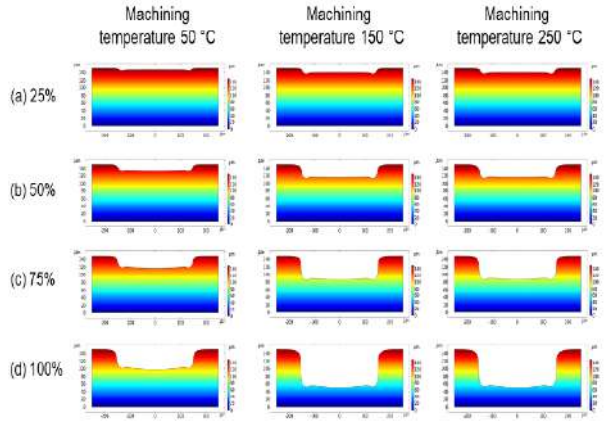

Figure 5. Cavity depth of the machined cavities (a) 25 %, (b) 50 %, (c) 75 % and (d) 100 % at 50, 150 and 250 °C.

Figure 6 shows the 3D temperature profile distribution of the cavities at 50, 150, 250 °C. The temperature profile shows the heat transfer process inside the cavity against the temperature scale, was red, of which the highest top layer indicated a value of about 1400 °C, which is the Si's melting point temperature. This means that the melting point had been reached and was able to remove the workpiece during the sparking. Figure 6(a-d) represents the workpiece's temperature profile after quarter, half, three-quarters, and the whole of removal of the layer. The temperature profile was simulated by applying the temperature to the workpiece's surface, and then removing it layer-by-layer, with the spark gap interval between the tool and the workpiece, set to about 5 µm. The machined profile at 100 % visualized each temperature setting, as the final cavity depth which could be achieved. The results proved that the machining temperature highly influenced the µEDM's performance in terms of the MRR.

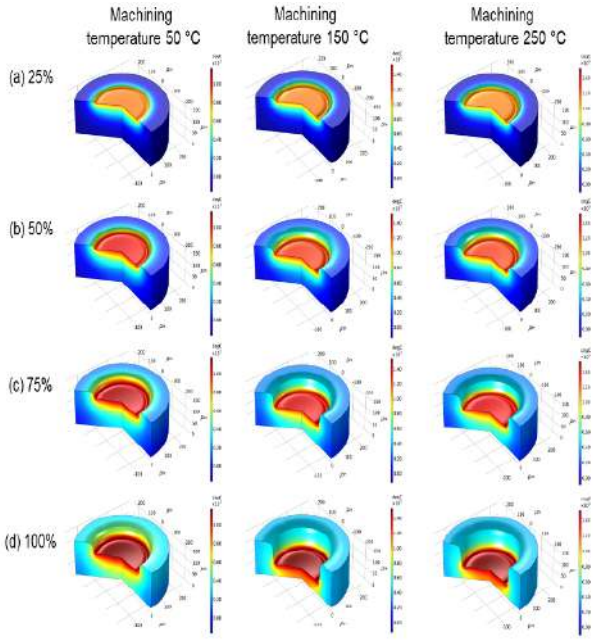

Figure 6. Temperature profile at (a) 50 °C (b) 150 °C and (c) 250 °C.

4. CONCLUSION

The dependence of the machining temperature on the MRR performances of heat-assisted μEDM was studied using numerical simulation analysis. The effect of the temperature on the cavity depth and temperature profile was analyzed for lightly doped Si wafer. The simulation results showed the machining temperature gives significant results on the heat transfer process. The 3D images of machined cavities on temperature profile with varying temperature and depth removes due to different machined volume. The machined cavities with different machining temperature (100, 150, 200 and 250 °C) showed full removal of 100 μm depth except for 30 and 50 °C, which concluded as not allowable temperature for the heat-assisted μEDM setup. The novel numerical simulation of Si machining on MRR results helps to improve the quality of the μEDM machining applications.

ACKNOWLEDGMENT

This research was funded by Universiti Teknologi Malaysia under Industry-International Incentive Grant (IIIG Q.J130000.3651.02M36). Noor Dzulaikha thank the Ministry of Higher Education Malaysia for MyBrain15 scholarship.

REFERENCES

[1] J. Murray, M. Fay, M. Kunieda, and A. Clare, "TEM study on the electrical discharge machined surface of single-crystal silicon," *Journal of Materials Processing Technology,* vol. 213, no. 5, pp. 801-809, 2013.

[2] J. Punturat, V. Tangwarodomnukun, and C. Dumkum, "Surface characteristics and damage of monocrystalline silicon induced by wire-EDM," *Applied Surface Science,* vol. 320, pp. 83-92, 2014.

[3] Q. Mingbo, L. Zhidong, T. Zongjun, W. Wei, and H. Yinhui, "Study of unidirectional conductivity on the electrical discharge machining of semiconductor crystals," *Precision Engineering,* vol. 37, no. 4, pp. 902-907, 2013.

[4] Y. K. Madhukar, S. Mullick, and A. K. Nath, "A study on co-axial water-jet assisted fiber laser grooving of silicon," *Journal of Materials Processing Technology,* vol. 227, pp. 200-215, 1// 2016.

[5] A. Belyaev, O. Polupan, W. Dallas, S. Ostapenko, D. Hess, and J. Wohlgemuth, "Crack detection and analyses using resonance ultrasonic vibrations in full-size crystalline silicon wafers," *Applied physics letters,* vol. 88, no. 11, p. 111907, 2006.

[6] N. Hung, Y. Fu, and M. Y. Ali, "Focused ion beam machining of silicon," *Journal of materials processing technology,* vol. 127, no. 2, pp. 256-260, 2002.

[7] D. Reynaerts, W. Meeusen, and H. Van Brussel, "Machining of three-dimensional microstructures in silicon by electro-discharge machining," *Sensors and Actuators A: Physical,* vol. 67, no. 1, pp. 159-165, 1998.

[8] M. P. Jahan, T. Lieh, Y. San Wong, and M. Rahman, "An experimental investigation into the micro-electrodischarge machining behavior of p-type silicon," *The International Journal of Advanced Manufacturing Technology,* vol. 57, no. 5-8, pp. 617-637, 2011.

[9] N. D. Daud, A. AbuZaiter, P. L. Leow, and M. S. M. Ali, "The effects of the silicon wafer resistivity on the performance of microelectrical discharge machining," *The International Journal of Advanced Manufacturing Technology,* vol. 95, no. 1-4, pp. 257-266, 2018.

[10] A. Bilal, M. Jahan, D. Talamona, and A. Perveen, "Electro-Discharge Machining of Ceramics: A Review," *Micromachines,* vol. 10, no. 1, p. 10, 2019.

[11] Y. Luo, C. Chen, and Z. Tong, "Investigation of silicon wafering by wire EDM," *Journal of materials science,* vol. 27, no. 21, pp. 5805-5810, 1992.

[12] M. Kunieda and S. Ojima, "Improvement of EDM efficiency of silicon single crystal through ohmic contact," *Precision engineering,* vol. 24, no. 3, pp. 185-190, 2000.

[13] T. Saleh, A. N. Rasheed, and A. G. Muthalif, "Experimental study on improving μ-WEDM and μ-EDM of doped silicon by temporary metallic coating," *The International Journal of Advanced Manufacturing Technology,* vol. 78, no. 9-12, pp. 1651-1663, 2015.

[14] N. D. Daud *et al.*, "Heat-assisted μ-electrical discharge machining of silicon," *The International Journal of Advanced Manufacturing Technology,* pp. 1-12, 2021.

[15] S. S. Mujumdar, D. Curreli, S. G. Kapoor, and D. Ruzic, "Modeling of melt-pool formation and material removal in micro-electrodischarge machining," *Journal of Manufacturing Science and Engineering,* vol. 137, no. 3, 2015.

[16] M. R. Patel, M. A. Barrufet, P. T. Eubank, and D. D. DiBitonto, "Theoretical models of the electrical discharge machining process. II. The anode erosion model," *Journal of applied physics,* vol. 66, no. 9, pp. 4104-4111, 1989.

[17] M. Singh, P. Saxena, J. Ramkumar, and R. Rao, "Multi-spark numerical simulation of the micro-EDM process: an extension of a single-spark numerical study," *The International Journal of Advanced Manufacturing Technology,* vol. 108, no. 9, pp. 2701-2715, 2020.